BIOCHEMISTRY
including biophysical chemistry & molecular biology

Article

pubs.acs.org/biochemistry

Lipid Selectivity, Orientation, and Extent of Membrane Binding of Nonacylated RP2

Éric Demers,[†] Élodie Boisselier,[†] Habib Horchani,[†] Daniel Blaudez,[‡] Philippe Calvez,[†] Line Cantin,[†] Nicolas Belley,[†] Sophie Champagne,[†] Bernard Desbat,[‡] and Christian Salesse*[,†]

[†]CUO-Recherche, Hôpital du Saint-Sacrement, Centre de recherche du CHU de Québec and Département d'ophtalmologie, Faculté de médecine, and Regroupement stratégique PROTEO, Université Laval, Québec, Québec, Canada

[‡]CBMN-UMR 5248 CNRS, Université de Bordeaux, IPB, Allée Geoffroy Saint Hilaire, 33600 Pessac, France

Supporting Information

ABSTRACT: Retinitis pigmentosa 2 (RP2) is an ubiquitary protein of 350 residues. The N-terminus of RP2 contains putative sites of myristoylation and palmitoylation. The dually acylated protein is predominantly localized to the plasma membrane. However, clinically occurring substitution mutations of RP2 in photoreceptors lead to the expression of a nonacylated protein, which was shown to be misrouted to intracellular organelles using different cell lines. However, the parameters responsible for the modulation of the membrane binding of nonacylated RP2 (naRP2) are still largely unknown. The maximal insertion pressure of naRP2 has thus been determined after its injection into the subphase underneath monolayers of phospholipids, which are typical of photoreceptor membranes. These data demonstrated that naRP2 shows a preferential binding to saturated phospholipid monolayers. Moreover, polarization modulation infrared reflection absorption spectroscopy has allowed comparison of the secondary structure of this protein in solution and upon binding to phospholipid monolayers. In addition, simulations of these spectra have allowed to determine that the β-helix of naRP2 has an orientation of 60° with respect to the normal, which remains unchanged regardless of the type of phospholipid. Finally, ellipsometric measurements of naRP2 demonstrated that its particular affinity for saturated phospholipids can be explained by its larger extent of insertion in this phospholipid monolayer compared to that in polyunsaturated phospholipid monolayers.

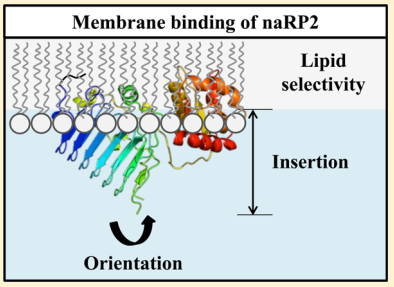

Retinitis pigmentosa 2 (RP2) is a ubiquitary protein of 350 amino acids.[1] Its crystal structure has revealed two main domains: the N- and C-terminal domains consist of a β-helix (amino acids 1−228) and of α-helices and β-sheets (amino acids 229−350),[2] respectively (Figure S1 of the Supporting Information). The sequences of the N- and C-terminal domains are 30% identical with that of cofactor C, a tubulin-specific chaperone,[1,3] and 34% identical with that of nucleoside diphosphate kinase, respectively.[3,4] The function of RP2 has not yet been fully clarified. It has, however, been clearly shown to function as a GTPase-activating protein of ADP-ribosylation factor-like 3 (Arf-like 3 or Arl3).[5] Phosphodiesterase 6 δ (PDE6δ) and Uncoordinated 119 protein (Unc119) cooperate with Arl3 to regulate the membrane association of lipid-modified proteins.[6] The stimulation of GTPase activity of Arl3 by RP2 results in the release of Unc119 from Arl3.[7] RP2 may play several roles in regulating the transport of lipid-modified proteins.[8−13]

Putative sites for myristoylation and palmitoylation have been identified at the N-terminus of RP2 on glycine 2 and cysteine 3, respectively.[14] The localization of RP2 to the ciliary apparatus at the base of the photoreceptor cilium was shown to be dependent on its N-terminal myristoylation.[8] In contrast, N-terminal myristoylation and palmitoylation are necessary to localize RP2 to the plasma membrane of the rod photoreceptor inner segment as well as to the very tips of the outer segment.[8,15,16] It was also shown to be located to the plasma membrane of different types of cultured cells[14,17−19] and of the cells throughout the retina.[16] Moreover, its binding to Arl3 was found to be favored with nonacylated RP2.[3] The clinically occurring mutations of RP2 are distributed all along its primary sequence.[1,20−23] However, the G2V, C3S, and ΔS6 mutations of RP2 are greatly important because they modify its acylation and thus disrupt its plasma membrane targeting.[14,17−19] In fact, cytoplasmic and nuclear staining was seen upon transfection of nonacylated RP2 (G2A, G2A/C3S, and ΔS6 mutants) using CHO[14] and HeLa[19] cell lines, whereas exclusively cytoplasmic staining was observed for the myristoylated C3S-RP2 mutant.[14] These data were quite consistent with the Western blot analyses of the subcellular fractionation of these cell lines.[14,19] Moreover, the use of an inhibitor of acylation in SH-SY5Y cell lines resulted in the distribution of nonacylated RP2 to intracellular organelles and the cytoplasm, thereby strongly suggesting that nonacylated RP2 binds intracellular membranes.[18] Altogether, most data agree that nonacylated RP2 is misrouted to the membranes of intracellular organelles. It is

Received: December 13, 2014
Revised: April 3, 2015
Published: April 6, 2015

DOI: 10.1021/bi501517r
Biochemistry 2015, 54, 2560−2570

therefore important to characterize the membrane binding properties of nonacylated RP2 (naRP2).

This work was thus performed to gain biophysical information about naRP2 membrane binding properties and selectivity for particular phospholipids using the monolayer model membrane system. There is a direct thermodynamic relationship between monolayers and bilayers.[24−26] Phospholipid monolayers are very useful model membranes as this method allows the control of several physical parameters such as the density of lipids and the surface pressure, the subphase content, the lipid composition, etc.[24,27−35] Lipid monolayers are very well suited to study membrane binding of peripheral proteins, in particular for acylated proteins. Indeed, peripheral proteins do not protrude deeper in the bilayer than one monolayer leaflet. It has thus been extensively used to study lipid−protein and lipid−peptide interactions (for recent reviews, see refs 36−40).

The outer segments of photoreceptor membranes have a unique characteristic in that they are the most unsaturated natural membranes discovered to date.[41] Indeed, more than 60% of their fatty acyl chains are polyunsaturated.[42,43] This is also true for the rod inner segment and the synaptic terminal.[44,45] These membranes contain three main fatty acyl chains: docosahexaenoic (22:6ω3), palmitic (16:0), and stearic (18:0) acids.[42,43] Moreover, detergent-resistant membranes (DRMs) comprise 8% of total photoreceptor lipids,[46] and nearly 65% of their phospholipid fatty acyl chains are saturated with a predominance of palmitic and stearic acids.[47] A significant proportion of RP2 was also shown to be associated with DRMs in photoreceptors[48] and in different types of cultured cells.[17] Measurements of naRP2 membrane binding in monolayers have thus been performed using the major phospholipids that can be found in photoreceptor membranes.

MATERIALS AND METHODS

Materials. The deionized water used for the preparation of buffer solutions was from a Barnstead Nanopure system (Barnstead, Dubuque, IA). Its resistivity and surface tension at 20 °C were 18.2 MΩ cm and 72 mN/m, respectively. Phospholipids were from Avanti Polar Lipids (Alabaster, AL): dimyristoylphosphocholine (DMPC), dipalmitoylphosphocholine (DPPC), distearoylphosphocholine (DSPC), didocosahexaenoylphosphocholine (DDPC), palmitoyldocosahexaenoylphosphocholine (PDPC), stearoyldocosahexaenoylphosphocholine (SDPC), dipalmitoylphosphoethanolamine (DPPE), distearoylphosphoethanolamine (DSPE), didocosahexaenoylphosphoethanolamine (DDPE), dipalmitoylphosphoserine (DPPS), distearoylphosphoserine (DSPS), and didocosahexaenoylphosphoserine (DDPS). $MgCl_2$ and ultrapure NaCl (99.9%) were purchased from J. T. Baker (Phillipsburg, NJ). β-Mercaptoethanol was from Sigma (St. Louis, MO). High-grade sodium phosphates were from Merck (Darmstadt, Germany), and Tris-HCl was from the Laboratoire Mat (Quebec, QC). The resin used for protein purification was from GE Healthcare (Buckinghamshire, England). All chemicals were used as received. Rod outer segment (ROS) lipids were extracted as described by Miljanich et al.[43] using ROS isolated by the method of Yamazaki et al.[49] using fresh retina obtained from a local slaughterhouse. All experiments were performed at least twice with reproducible results.

Expression and Purification of naRP2. The RP2 construct (amino acids 1−350) cloned in plasmid pGEX-4T3 to express a GST fusion protein was a kind gift from A. Wittinghofer (Max-Planck-Institut für Molekulare Physiologie, Dortmund, Germany). The protein was expressed and purified as described previously.[50] Briefly, naRP2 was expressed in *Escherichia coli* Bl21(DE3) RIPL for 5 h at 37 °C. Bacteria were then pelleted by centrifugation and stored at −20 °C. The protocol used for the purification of naRP2 was a modification of the method previously described by Kühnel et al.[2] Pellets were resuspended in load buffer [50 mM Tris (pH 7.4), 100 mM NaCl, 5 mM $MgCl_2$, and 3 mM β-mercaptoethanol] at 4 °C. Bacterial lysis was conducted by sonication followed by centrifugation at 20000*g* for 1 h. The cell lysate supernatant was loaded on a GSTrap column preequilibrated with the load buffer. The column was washed with 10 column volumes of load buffer. Then, GST was cleaved with thrombin overnight at 4 °C directly on the column. A HiTrap Benzamidine FF (high sub) column equilibrated with a modified load buffer containing 500 mM NaCl was located directly after the GSTrap column to eliminate thrombin. Elution of naRP2 was performed with the modified load buffer. The eluted naRP2 was then concentrated by ultrafiltration with an Amicon Ultra 15 filter (Millipore), during which buffer was changed to that used for its storage [5 mM phosphate (pH 7.4) and 3 mM β-mercaptoethanol]. naRP2 was kept at 4 °C until being used. The purity of naRP2 was at least 99% as judged by gel electrophoresis with Coomassie blue staining. Sequence identity was confirmed by mass spectrometry analysis by the Service de protéomique of the Centre de recherche du CHU de Québec.

Monolayer Binding Parameters of naRP2. A home-built round Teflon trough (diameter, 20 mm; depth, 2 mm) filled with 1200 μL of monolayer buffer [5 mM phosphate (pH 7.4) and 100 mM NaCl] was used for the monolayer measurements. The experimental setup was placed in a Plexiglas box with humidity control at 21 ± 1 °C. A phospholipid monolayer was formed by spreading a few microliters of a solution of phospholipids solubilized in an organic solvent until the desired initial surface pressure (Π_i) was reached. The waiting time period for spreading solvent evaporation and for the film to reach equilibrium varied with spreading volume, initial surface pressure, and lipid concentration. naRP2 was then injected underneath this monolayer to reach a protein concentration of 20 μg/mL. The kinetics of binding of naRP2 to the phospholipid monolayer was monitored until equilibrium was reached (typically for 3 h) using a surface pressure detector. Surface pressure (Π) was measured by the Wilhelmy method using a microbalance (Nima technology, Coventry, U.K.) connected to a computer. A surface pressure increase, $\Delta\Pi$ ($\Delta\Pi = \Pi_e - \Pi_i$), is observed after the injection of naRP2 into the subphase, where Π_e is the surface pressure at equilibrium.

The determinations of the maximal insertion pressure (MIP) and of the synergy were shown to be very useful for comparing extent of protein binding to different lipid monolayers.[29,50] The MIP values have been determined by extrapolating the plot of $\Delta\Pi$ at equilibrium as a function of Π_i where the linear regression reaches a value of 0 on the *x*-axis.[50] MIP values have been obtained for the binding of naRP2 to different lipid monolayers. Measurements with the polyunsaturated phospholipids were performed under either nitrogen, argon, or atmospheric air, but no difference was observed among these different conditions as previously assayed.[51] The details of the calculation of the uncertainty of the MIP were given by Calvez et al.[29] Briefly, the uncertainty, which depends on the number

DOI: 10.1021/bi501517r
Biochemistry 2015, 54, 2560−2570

of experimental points as well as on the quality of the fit of the regression curve, was calculated from the covariance of the experimental data on the linear regression. The synergy value corresponds to the slope of the linear regression of the plot of Π_e as a function of Π_i.[50] It can also be obtained by adding 1 to the slope of the linear regression of $\Delta\Pi$ as a function of Π_i.[52] We have previously shown that a negative synergy indicates an unfavorable binding of the protein to the phospholipid monolayer, whereas a positive synergy reveals a favorable binding. Values of synergy close to zero suggest that there is neither attraction nor repulsion between the protein and the monolayer.[50] The uncertainty of the synergy is calculated using the term $[\sigma(\Pi_e)(1 - r^2)^{1/2}]/[\sigma(\Pi_i)(n - 2)^{1/2}]$, where σ is the standard deviation, r is the correlation coefficient, and n is the number of points. We have recently created a freely available webpage where these binding parameters and experimental errors can be readily calculated (http://www.crchudequebec.ulaval.ca/BindingParametersCalculator/).

Measurement of Infrared Spectra of naRP2. Infrared spectra of naRP2 in solution were measured with a Golden Gate ATR accessory (Specac, Woodstock, NY) installed in a Thermo Nicolet 6700 Fourier transform infrared (FTIR) spectrometer. The spectrum of the buffer was subtracted from that of naRP2 to obtain the spectrum of the pure protein. Polarization modulation infrared reflection absorption spectroscopy (PM-IRRAS) was performed using a Nicolet Nexus 870 FTIR instrument as previously described.[53−55] Briefly, PM-IRRAS combines Fourier transform mid-IR reflection spectroscopy with rapid polarization modulation of the incident beam.[55] Each PM-IRRAS spectrum was the result of the co-addition of 600 scans at a resolution of 8 cm^{-1}. A home-built round Delrin trough (diameter, 60 mm; depth, 1 mm) filled with 4.5 mL of monolayer buffer and a protein concentration of 20 μg/mL were used for these experiments at a constant area. To remove the isotropic contributions from bulk water and water vapor, experimental drifts, and the dependence on the Bessel function, the spectrum of naRP2 in the presence of the phospholipid monolayer was divided by that of the pure phospholipid monolayer to produce the resulting normalized PM-IRRAS spectrum. Similarly, the spectrum of the pure naRP2 monolayer was obtained by dividing the PM-IRRAS spectrum of the protein by that of the subphase buffer. In these experiments, the monolayer buffer was prepared with either H_2O or D_2O. Experiments were performed at 21 ± 0.5 °C. The maximum of the infrared bands has been determined by using the second derivative (or Fourier deconvolution) to the spectra.

Simulations of the PM-IRRAS Spectra of naRP2. Simulated spectra have been obtained using a general software developed for modeling the reflectivity of absorbing layered systems[56] and extended to anisotropic systems following the matrix method of Berreman.[57] To determine the orientation of naRP2 on H_2O and D_2O buffers from the PM-IRRAS spectra, simulations were performed by generating the optical constants of the various secondary structures from previously published or determined data in water.[58,59] The frequencies of the amide I maxima of the various structures are listed in Table 1.[60−65] For all structures, the k_{max} isotropic intensity of the amide I band was fixed to 0.4 with $k_{iso} = (k_x + k_y + k_z)/3$. The optical index of the deuterium-exchanged structures was obtained by shifting the maximum of each structure to a low frequency in accordance with previously published data.[63] The amide I maxima of the secondary structures exchanged with D_2O are also listed in Table 1. The bandwidth was set to 30 cm^{-1}. The simulated PM-IRRAS spectra were obtained by performing the summation of the spectrum of each individual secondary structure when taking into account their proportion and their respective orientation in the known structure of RP2 (Figure S1 of the Supporting Information).[2] The baseline was corrected in all spectra, and the simulated spectral intensity was normalized with respect to that of the experimental amide I intensity.

Table 1. Frequencies of Amide I of the Various Secondary Structures Used for the Simulations of the PM-IRRAS Spectra of RP2 in H_2O and D_2O

structure	H_2O (cm^{-1})	D_2O (cm^{-1})
α-helix	1654	1649
β-helix	1638	1633
β-sheet	1629, 1684[a]	1626, 1679[a]
β-turn	1672	1671
random coil	1648	1636

[a]This minor absorption band for antiparallel β-sheets is typically difficult to observe by PM-IRRAS because of its weak nature.

Ellipsometric Measurements. The ellipsometric angles (Δ and ψ) and surface pressure (Π) were recorded simultaneously with the same trough. The ellipsometric measurements were taken with a conventional null ellipsometer using a He−Ne laser operating at 632.8 nm, which is similar to that described elsewhere.[66,67] The angle of incidence was 52.12° (the Brewster angle of the air−water interface for pure water is 53.12°). A home-built round Teflon trough (diameter, 60 mm; depth, 5 mm) filled with 10 mL of monolayer buffer has been used for these experiments at a constant area. The surface pressure was measured with a Nima PS4 film balance using the Wilhelmy method. All experiments were performed at 20 ± 1 °C. The protein concentration in the subphase was 20 μg/mL.

RESULTS AND DISCUSSION

naRP2 Binds More Selectively to Phospholipids with Saturated Fatty Acyl Chains. The optimal concentration of naRP2 for the monolayer measurements was estimated by injecting different amounts of naRP2 underneath a monolayer of DMPC at a Π_i of 5 mN/m. $\Delta\Pi$ was then monitored as a function of time until equilibrium was reached. An optimal naRP2 concentration of 20 μg/mL was chosen as it corresponds to the onset of monolayer saturation.

The MIP of a protein is a valuable tool for determining the extent of binding of protein to lipid monolayers.[29,50,68] It corresponds to the maximal surface pressure up to which naRP2 can insert into the monolayer and beyond which no insertion takes place. Figure 1 shows a typical example of the determination of the MIP of naRP2. As can be seen in the inset of Figure 1, the larger is the initial surface pressure and the smaller the increase in surface pressure ($\Delta\Pi$). Indeed, $\Delta\Pi$ values of 14.0, 11.8, 6.2, 4.2, and 1.6 mN/m have been obtained for Π_i values of 5.2, 10.5, 15.8, 20.5, and 24.9 mN/m, respectively. A negative slope is thus obtained when plotting these values of $\Delta\Pi$ as a function of Π_i (Figure 1), which allowed calculation of a MIP value of 27.2 ± 1.4 mN/m for naRP2 in the presence of SDPC. The slope of this plot provides information about the synergy between this protein and the phospholipid monolayer. Briefly, the synergy is >0 when a positive interaction between the protein and the lipids is observed, whereas the synergy is <0 when a repulsion between the protein and the lipid monolayer is observed.[50] In the case of

DOI: 10.1021/bi501517r
Biochemistry 2015, 54, 2560−2570

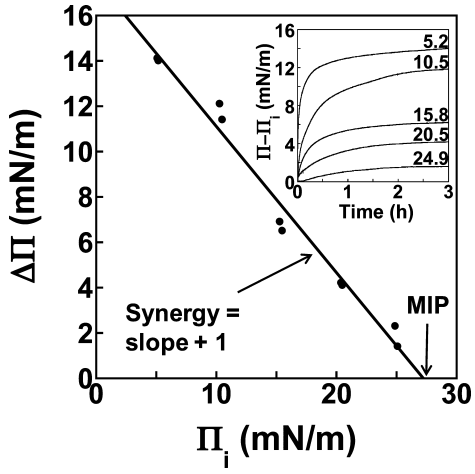

Figure 1. Typical example of the determination of the binding parameters of naRP2 to a SDPC monolayer. The maximal insertion pressure (MIP) is determined by extrapolating the plot of $\Delta\Pi$ as a function of the initial surface pressure (Π_i) where the curve reaches a value of 0 on the *x*-axis. The synergy is calculated by adding 1 to the slope of this plot. The inset shows typical kinetics of binding of naRP2 to the SDPC monolayer at different Π_i values of 5.2, 10.5, 15.8, 20.5, and 24.9 mN/m as a function of the time until equilibrium (Π_e) is reached (only a few kinetics are shown for the sake of clarity). The initial surface pressure was subtracted from the increase in surface pressure ($\Pi - \Pi_i$) and plotted as a function of time.

SDPC (Figure 1), a synergy of 0.36 ± 0.03 has been obtained, thus suggesting that a positive interaction takes place between naRP2 and this lipid monolayer. Different values of MIP and synergy can be obtained depending on naRP2 surface activity and its affinity for given lipid monolayers.

Extensive binding parameter measurements have thus been performed with the major phospholipids found in ROS membranes that mainly contain phosphoethanolamine (45%), phosphocholine (38%), and phosphoserine (14%).[69] Moreover, palmitoyl (C16:0), stearoyl (C18:0), and docosahexaenoyl (C22:6ω3) are the main fatty acyl chains of ROS phospholipids (phosphoethanolamine, 10.7% C16:0, 22.3% C18:0, and 50.6% C22:6ω3; phosphocholine, 19.6% C16:0, 17.3% C18:0, and 41.9% C22:6ω3; phosphoserine, 1.2% C16:0, 18.2% C18:0, and 49.2% C22:6ω3[42]). Phospholipids bearing palmitoyl, stearoyl, or docosahexaenoyl fatty acyl chains have thus been used to study naRP2 monolayer binding. Moreover, varying amounts of ROS phospholipids contain one saturated and one polyunsaturated fatty acyl chain.[43] Therefore, PDPC and SDPC have also been used to determine the effect of such mixed fatty acyl chains on the behavior of naRP2 monolayer binding. In addition, binding parameter measurements have also been performed with an organic extract of total ROS lipids to mimic the whole lipid content of these membranes. The values of MIP and synergy are easier to compare when they are plotted as histograms.

The MIP and synergy values obtained with different phosphocholines are shown in Figures 2A and 3A, respectively. MIP values of 31.6 ± 2.0, 35.2 ± 2.2, 17.8 ± 1.6, 19.4 ± 0.4, and 27.2 ± 1.4 mN/m have been obtained for naRP2 in the presence of DPPC, DSPC, DDPC, PDPC, and SDPC, respectively (Figure 2A). Moreover, a value of 25.5 ± 1.2 mN/m has been obtained with total ROS lipids. The much larger values of MIP obtained in the presence of phosphocholines bearing two saturated fatty acyl chains (DPPC and DSPC) compared to that of a phosphocholine with two polyunsaturated fatty acyl chains (DDPC) suggest that saturation of phospholipid fatty acyl chains favors naRP2 monolayer binding, whereas unsaturation leads to unfavorable binding. This result is supported by the values of synergy obtained for these three phosphocholines: 0.44 ± 0.05, 0.43 ± 0.03, and −0.15 ± 0.1 for DPPC, DSPC, and DDPC, respectively (Figure 3A). Indeed, there is a strong positive synergy between the phosphocholines bearing two saturated fatty acyl chains, whereas a repulsion is observed between the polyunsaturated DDPC and naRP2. In the case of DDPC, it would be more appropriate to refer to an exclusion pressure rather than a MIP.[50] Indeed, the MIP obtained with a synergy of <0 could be called "exclusion pressure" because it corresponds to a repulsion between the protein and the monolayer. It is noteworthy that similar values of MIP have been obtained for DDPC and PDPC whereas a much larger MIP value has been observed for SDPC, which suggests that a sufficiently long saturated fatty acyl chain (C18:0) favors naRP2 monolayer binding even when the other fatty acyl chain is the polyunsaturated docosahexaenoyl (C22:6ω3). The values of synergy also illustrate this trend. Indeed, a much larger synergy value of 0.36 ± 0.03 has been observed for SDPC compared to the small positive value obtained for PDPC (0.14 ± 0.02). These data further support the idea that phospholipids with saturated fatty acyl chains favor naRP2 monolayer binding, as previously postulated.[17,48] In addition, the values of MIP obtained with DPPC and DSPC are larger than the estimated membrane lateral pressure (~30 mN/m).[70−77] One could thus postulate that naRP2 can bind

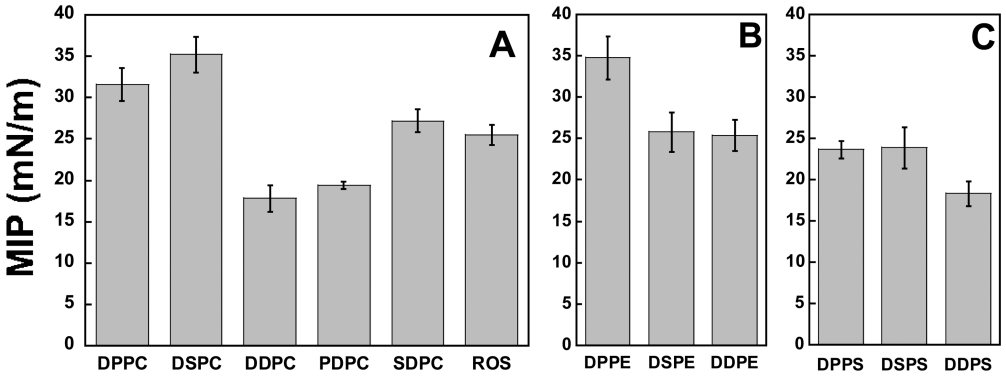

Figure 2. Maximal insertion pressures of naRP2 in the presence of different phospholipid monolayers: (A) DPPC, DSPC, DDPC, PDPC, SDPC, and total bovine rod outer segment (ROS) lipids; (B) DPPE, DSPE, and DDPE; and (C) DPPS, DSPS, and DDPS.

DOI: 10.1021/bi501517r
Biochemistry 2015, 54, 2560−2570

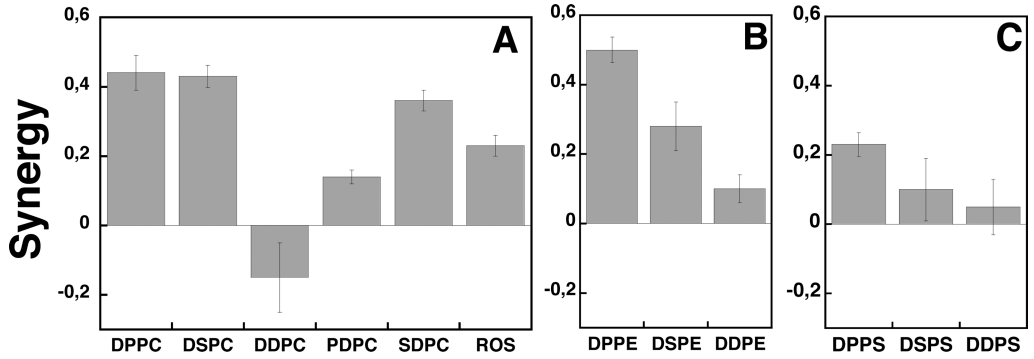

Figure 3. Synergy of naRP2 in the presence of different phospholipid monolayers: (A) DPPC, DSPC, DDPC, PDPC, SDPC, and total bovine rod outer segment (ROS) lipids; (B) DPPE, DSPE, and DDPE; and (C) DPPS, DSPS, and DDPS.

these saturated phospholipids in ROS cell membranes but more likely if they gather together such as in microdomains.

Figures 2B and 3B show the MIP and synergy values, respectively, obtained with different phosphoethanolamines. MIP values of 34.8 ± 2.6, 25.8 ± 2.4, and 25.4 ± 1.9 mN/m have been obtained for naRP2 in the presence of DPPE, DSPE, and DDPE, respectively (Figure 2B). A much larger MIP value has been obtained with DPPE, which is larger than the estimated membrane lateral pressure. Moreover, a much larger synergy value of 0.5 ± 0.04 has been obtained with DPPE compared to 0.28 ± 0.07 for DSPE and to the very small value of 0.1 ± 0.04 for DDPE (Figure 3B). These data suggest that naRP2 monolayer binding is more favored in the presence of phosphoethanolamine with shorter saturated fatty acyl chains.

The MIP and synergy values obtained with different phosphoserines are shown in Figures 2C and 3C, respectively. MIP values of 23.7 ± 1.1, 23.9 ± 2.5, and 18.4 ± 1.5 mN/m have been obtained for naRP2 in the presence of DPPS, DSPS, and DDPS, respectively (Figure 2C). Slightly larger values of MIP have been obtained in the presence of phosphoserines bearing two saturated fatty acyl chains (DPPS and DSPS) than in the presence of phosphoserines bearing two polysaturated (DDPS) fatty acyl chains. Moreover, the values of synergy are 0.23 ± 0.03, 0.1 ± 0.09, and 0.05 ± 0.08 for DPPS, DSPS, and DDPS, respectively (Figure 3C). These values of synergy and MIP, which are much lower than the estimated membrane lateral pressure, suggest that the negative charge of phosphoserine disfavors membrane binding of naRP2.

ROS membranes contain a mixture of varying amounts of approximately nine different unsaturated phosphocholines, 18 different saturated−unsaturated phosphocholines, two different saturated phosphocholines, approximately nine different unsaturated phosphoethanolamines, 16 different saturated−unsaturated phosphoethanolamines, approximately two different saturated phosphoethanolamines, and approximately nine different unsaturated phosphoserines and approximately eight different saturated−unsaturated phosphoserines.[43] The MIP value of 25.5 mN/m and the synergy of 0.23 obtained with ROS lipids (Figures 2A and 3A) thus result from the binding of naRP2 to this complex mixture of phospholipids. The content of DPPC, DSPC, DPPE, and DSPE in this lipid mixture can be estimated to be ∼9% of total phospholipids, whereas more than 50% of ROS phospholipids contain one polyunsaturated fatty acyl chain (PDPC, SDPC, DDPC, PDPE, SDPE, DDPE, SDPS, and DDPS).[43] The smaller value of MIP obtained with the ROS lipid mixture (25.5 mN/m) compared to the estimated membrane lateral pressure (∼30 mN/m) can thus be explained by the low content of saturated phosphocholines and phosphoethanolamines in ROS membranes. Altogether, these data suggest that naRP2 could be associated with microdomains in photoreceptor membranes, which are known to be enriched with phospholipids with saturated fatty acyl chains (mainly palmitic and stearic acids, such as in DPPC, DSPC, DPPE, and DSPE).[47]

Given that very large differences have been observed between the binding parameters of naRP2 in the presence of DSPC and DDPC, infrared spectroscopic and ellipsometric measurements have been performed using these phospholipids to explain the influence of phospholipid saturation and unsaturation on naRP2 membrane binding.

Secondary Structure of naRP2 in Monolayers. Infrared spectroscopy is very useful for gaining molecular information about the secondary structure and orientation of proteins during their binding to phospholipid monolayers.[27,36,78−81] The spectrum of naRP2 in solution was thus compared to that in a monolayer (Figure 4). To the best of our knowledge, those are the first infrared spectra of RP2. Two components can be seen in the amide I band of the PM-IRRAS spectrum of naRP2 in the absence of a lipid monolayer. The strongest one is centered at 1654 cm^{-1}, which can been attributed to α-helices[82,83] such as those located in both the N- and C-terminal domains of this protein (Figure S1 of the Supporting Information). In addition,

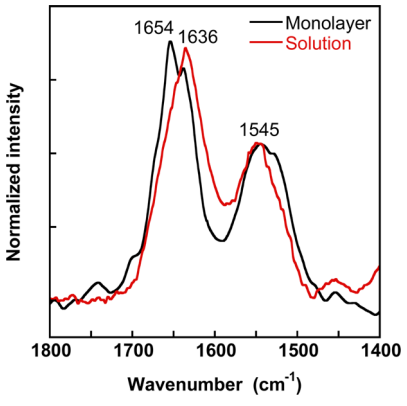

Figure 4. Comparison between the infrared spectra of naRP2 in solution and in monolayer. The spectrum of naRP2 in solution [5 mM phosphate (pH 7.4) and 3 mM β-mercaptoethanol in H_2O] measured using the Golden Gate ATR accessory is compared to that of naRP2 in the monolayer measured by PM-IRRAS using a subphase containing 5 mM phosphate (pH 7.4) and 100 mM NaCl in H_2O at a surface pressure of 12.6 mN/m.

DOI: 10.1021/bi501517r
Biochemistry 2015, 54, 2560−2570

the shoulder at 1636 cm^{-1} can been assigned either to the β-sheets of the C-terminal domain or to the β-helix of the N-terminal domain of RP2 (Figure S1 of the Supporting Information).[2] Indeed, the amide I band of β-sheets is typically located between 1630 and 1640 cm^{-1},[60,62,64,65] whereas that of the β-helix can be found between 1638 and 1644 cm^{-1}.[84] The amide I band of the spectrum of naRP2 in solution is centered at 1636 cm^{-1} (Figure 4), thus revealing the large contribution of the β-helix and the β-sheet components of the structure of RP2 to its amide I band (Figure S1 of the Supporting Information). The width of this band also includes the component corresponding to α-helices.[2] In contrast, the particular orientation of naRP2 in the monolayer in the absence of lipids most likely allows the observation of its secondary structure components from its amide I band.

Figure 5 shows the experimental and simulated PM-IRRAS spectra of naRP2 in the presence of monolayers of DDPC and DSPC. Figure 5A compares the spectrum of naRP2 in the presence and absence of a monolayer of DDPC. It can be seen that these two spectra are very similar. In the presence of DDPC, the amide I band of naRP2 includes components at 1653 and 1635 cm^{-1}, which correspond to the α-helical and β-helical and β-sheet structural elements of this protein, respectively, as described above (Figure 4). Therefore, the naRP2 secondary structure and orientation remain unchanged in the presence and absence of the DDPC monolayer.

PM-IRRAS spectra were more difficult to obtain in the presence of a DSPC monolayer. Indeed, infrared spectra of naRP2 in the presence of DSPC could be observed only when the buffer was prepared with D_2O. Figure S2 of the Supporting Information shows PM-IRRAS spectra before and after the injection of naRP2 into the H_2O subphase of a monolayer of DSPC. The three most intense bands in the spectrum of pure DSPC have been attributed to the υC═O ester stretching band at 1735 cm^{-1}, the δCH_2 bending mode at 1469 cm^{-1}, and the υ_aP═O mode at 1228 cm^{-1}. The position of these bands remains unchanged upon naRP2 binding except for the broad negative infrared band in the 1700−1640 cm^{-1} region that has been previously documented.[85] In brief, the water absorption band is centered at approximately 1640 cm^{-1}, which corresponds to the position at which the PM-IRRAS spectrum changes abruptly showing a positive band followed immediately by a negative band. This behavior is due to an abrupt variation of the refractive index of the aqueous subphase in this frequency range. The observation of a much more negative band in the presence of naRP2 can be attributed to a large perturbation of the refractive index of water in the vicinity of the polar head of DSPC. No amide I band could be observed in Figure S2 (Supporting Information) or when the spectrum of the naRP2−DSPC monolayer is divided by that of the pure DSPC monolayer. An amide I band of naRP2 could also not be observed in the presence of a DPPC monolayer on a H_2O subphase (data not shown). Measurements were thus attempted with a DSPC monolayer spread on a D_2O buffer subphase.

The PM-IRRAS spectrum of naRP2 injected underneath a DSPC monolayer into a D_2O buffer subphase can be seen in Figure 5B. A single component of the amide I band can be distinguished at 1633 cm^{-1}, which corresponds to the position attributed to the β-sheets of RP2 together with a contribution of its β-helix. No clear shoulder corresponding to the α-helices can be seen in this spectrum, although the width of this amide I band likely includes this component. The position of the

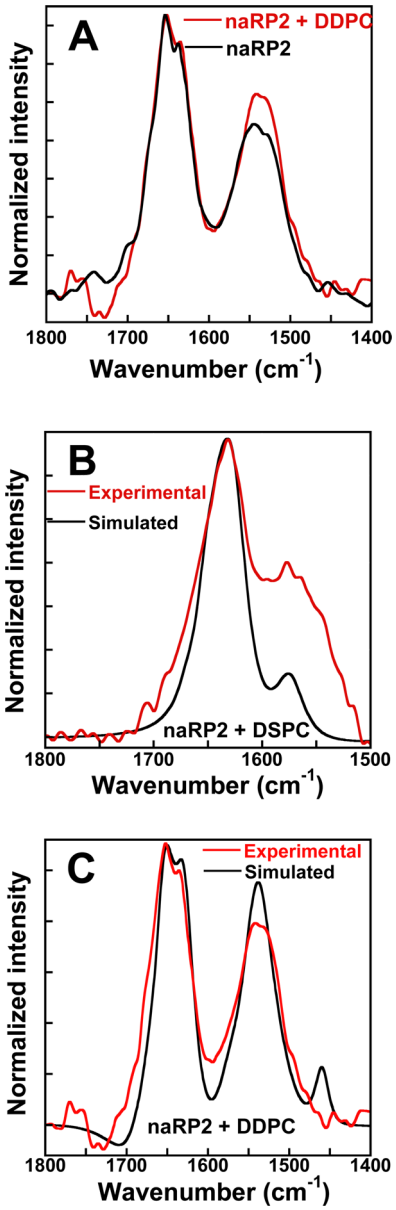

Figure 5. Comparison between the PM-IRRAS spectra of naRP2 in the absence and presence of DDPC and DSPC monolayers using a subphase containing 5 mM phosphate (pH 7.4) and 100 mM NaCl. (A) PM-IRRAS spectra of naRP2 alone and after binding to a DDPC monolayer in H_2O. (B) Experimental and simulated PM-IRRAS spectrum of naRP2 on a DSPC monolayer in D_2O. (C) Experimental and simulated PM-IRRAS spectrum of naRP2 in the presence of DDPC in H_2O (see panel A). The spectra were measured at surface pressures of 21.3 and 21.5 mN/m for DDPC and DSPC, respectively.

antisymmetric COO^- shoulder at 1576 cm^{-1} in D_2O can be attributed to the presence of the large number of aspartates and glutamates in RP2.[61,86] The difficulty in measuring a spectrum of naRP2 in the presence of DSPC compared to that in the presence of DDPC may reveal differences between the interaction of this protein with these phospholipid monolayers. This is consistent with the large differences observed between the values of MIP and synergy of naRP2 in the presence of DSPC and DDPC. These differences could be explained by changes either in the orientation or in the extent of penetration of naRP2 in these lipid monolayers. Simulations of the infrared

DOI: 10.1021/bi501517r
Biochemistry 2015, 54, 2560−2570

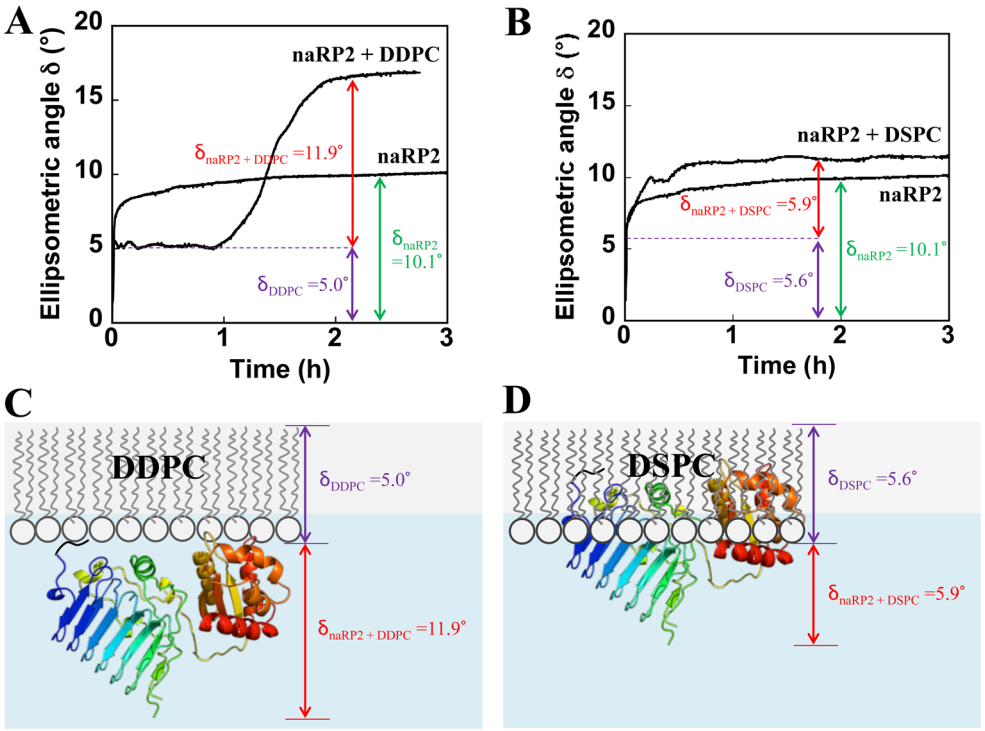

Figure 6. Ellipsometric isotherms of naRP2 binding in the absence and presence of (A) a DDPC monolayer and (B) a DSPC monolayer using a subphase containing 5 mM phosphate (pH 7.4) and 100 mM NaCl. The phospholipid monolayers were equilibrated at 5 mN/m prior to protein injection. The surface pressures at equilibrium were 21.7 and 21.3 mN/m for DDPC and DSPC, respectively. (C) Illustration of the orientation of naRP2 on the basis of the simulated PM-IRRAS spectra and extent of its insertion in the presence of a DDPC monolayer. (D) Illustration of the orientation and extent of insertion of naRP2 in the presence of a DSPC monolayer.

spectra and ellipsometric measurements have allowed clarification of these issues.

Estimation of the Orientation of naRP2 in Monolayers from the Simulation of the PM-IRRAS Spectra. It has previously been shown that it is possible to estimate the orientation of a protein upon comparison of experimental and simulated PM-IRRAS spectra.[87−89] The simulated spectrum showing the best agreement with the experimental spectrum of naRP2 in the presence of a DDPC monolayer on a H_2O subphase is shown in Figure 5C. It can indeed be seen that there is a very large overlap between the simulated and experimental spectra. The two components of the amide I band are located at almost the same position (1651 and 1634 cm^{-1} compared to 1653 and 1635 cm^{-1} for the simulated and the experimental spectra, respectively). The intensity of the amide II band of the simulated spectrum is slightly larger than that of the experimental spectrum, but their integrated intensity is very similar. Moreover, the amide II band of the simulated and experimental spectra is centered at nearly the same position (1539 and 1542 cm^{-1}, respectively). This simulated spectrum has been obtained using an orientation of 60° of the β-helix with respect to the normal, which allowed us to propose a specific orientation for naRP2 in our experiments (see a representation of this orientation of naRP2 in Figure 6B). This proposed orientation also takes into account an optimal orientation of the α-helices and β-sheets of the C-terminus of naRP2 (Figure S1 of the Supporting Information). Indeed, the orientation of these structural components must be close to parallel to the surface to obtain a large PM-IRRAS signal such as that observed in our experiments (Figure 5C).[89,90] This angle of 60° of the β-helix of naRP2 is close to the magic angle of 54.7°. Therefore, a distribution of different orientations of naRP2 around an angle of 60° cannot be excluded. Nevertheless, the large difference between the shape of the PM-IRRAS spectrum and that in solution (Figure 4) suggests a specific orientation of naRP2 in the monolayer. The same orientation has been obtained upon performance of the simulation of the spectrum of naRP2 in the presence of a DSPC monolayer on a D_2O subphase. As shown in Figure 5B, there is good agreement between the simulated and experimental amide I′ band of naRP2. The maximum of the amide I′ band of both spectra is observed at 1633 cm^{-1}. The only discrepancy between these two spectra lies in the difference in intensity in the region related to the absorption of individual amino acids, which is difficult to properly simulate. However, one can wonder how the very different spectra shown in panels B and C of Figure 5 can result in the same orientation of naRP2. A detailed analysis of the behavior of the individual structural components of naRP2 in the presence of H_2O and D_2O allowed us to provide an explanation for this observation. Indeed, one of the parameters responsible for the spectral differences observed in the presence of a H_2O and D_2O subphase is the presence of a large random coil secondary structure component in RP2. Indeed, RP2 contains 32% random coil, which results in a large amide I band intensity in H_2O. In the presence of H_2O, the maximum of the amide I band corresponding to a random coiled structure is centered almost exactly between that of α- and β-helices (Table 1). The α- and β-helical components of the amide I band can thus be observed because the baseline produced by the random coiled structure is equivalent in this range of frequencies. However, in the presence of D_2O, the position of the amide I band corresponding to random coils undergoes a much larger shift to lower wavenumbers than in the case of the α- and β-helical

DOI: 10.1021/bi501517r
Biochemistry 2015, 54, 2560−2570

structures or the β-sheets (Table 1). The maximum of this band then approaches that of the β-helix, which leads to an intense band at an intermediary wavenumber (1633 cm^{-1}) and to a rather large bandwidth, which likely includes the α-helical structure component.

The simulated PM-IRRAS spectra shown in panels B and C of Figure 5 thus allowed us to propose that naRP2 has the same orientation upon binding saturated (DSPC) or polyunsaturated (DDPC) phospholipid monolayers. This result does not therefore permit an explanation of the large differences observed between the binding parameters of naRP2 in the presence of these two phospholipids. Ellipsometric measurements have thus been performed to evaluate whether differences can be observed between the extent of penetration of the saturated or polyunsaturated phospholipid monolayer by naRP2.

Estimation of the Extent of Penetration of naRP2 in Saturated and Polyunsaturated Phospholipid Monolayers from Ellipsometric Measurements. The ellipsometric signal depends on both the refractive index and the thickness of the monolayer.[91] However, it can be assumed that it depends solely on monolayer thickness. Indeed, the measurement of an ellipsometric angle indicates that the interfacial layer has induced a phase change in the polarized light. In the case of a sufficiently dense film, the refractive index of this film is independent of the film thickness. Consequently, the observed phase change of such a dense film is proportional to the film thickness, as described previously for RPE65.[92] We thus assumed that pure naRP2 and the mixed naRP2−DDPC or naRP2−DSPC films have reached such a sufficiently high film density close to the end of their respective ellipsometric isotherm (or when equilibrium has been reached).

The evolution of the ellipsometric angle δ as a function of time upon binding of naRP2 in the absence and presence of a DDPC monolayer is presented in Figure 6A. In the absence of a phospholipid monolayer, an ellipsometric angle of 10.1° is obtained at equilibrium after naRP2 binding had proceeded for 3 h. The same experiments were performed in the presence of a DDPC monolayer, which contributes to the ellipsometric signal [δ_{DDPC} = 5.0° (see the dashed line in Figure 6A)]. Therefore, the ellipsometric signal upon binding of naRP2 to the DDPC monolayer starts at an ellipsometric angle δ of 5.0°. The ellipsometric signal obtained at equilibrium upon binding of naRP2 to the DDPC monolayer [11.9° + 5.0° = 16.9° (Figure 6A)] is slightly larger than the sum of the ellipsometric angle of naRP2 in the absence of a lipid monolayer [10.1° (Figure 6A)] and that of the pure DDPC monolayer (5.0°); i.e., 10.1° + 5.0° = 15.1°, as described by $\delta_{naRP2-DDPC} > \delta_{naRP2} + \delta_{DDPC}$. This observation thus suggests that the ellipsometric signal resulting from naRP2 binding approximately corresponds to the mere addition of the individual DDPC and naRP2 ellipsometric angles and thus that naRP2 is juxtaposed underneath the DDPC monolayer. naRP2 would thus weakly interact with the DDPC monolayer without penetrating this monolayer. A model depicting the proposed organization of the naRP2−DDPC monolayer using the orientation of naRP2 estimated from the simulated PM-IRRAS spectra is shown in Figure 6C. Moreover, a delay of approximately 1 h can be observed prior to the onset of the ellipsometric isotherm of naRP2 in the presence of DDPC (Figure 6A). In addition, the kinetics of the increase in the ellipsometric angle upon naRP2 binding in the presence of the DDPC monolayer is much slower than that in the absence of a lipid monolayer (Figure 6A) and that in the presence of DSPC (Figure 6B), thereby suggesting that naRP2 binds the polyunsaturated DDPC monolayer with very low affinity.

In contrast, naRP2 exhibits a completely different behavior in the presence of the DSPC monolayer. Indeed, the sum of the ellipsometric angle of naRP2 in the absence of a lipid monolayer [10.1° (Figure 6B)] and of the pure DSPC monolayer (δ_{DSPC} = 5.6°), i.e., 10.1° + 5.6° = 15.7°, is much larger than the ellipsometric signal obtained at equilibrium upon binding of naRP2 to the DSPC monolayer [5.6° + 5.9° = 11.5° (Figure 6B)], as described by $\delta_{naRP2} + \delta_{DSPC} > \delta_{naRP2-DSPC}$. In fact, a much smaller ellipsometric angle of approximately 5.9° is obtained for naRP2 at equilibrium, after subtraction of the contribution of pure DSPC (δ_{naRP2} = 11.5° − 5.6°), compared to the value of 10.1° observed for naRP2 in the absence of a lipid monolayer (Figures 6B). This significant decrease in δ in the presence of DSPC suggests that naRP2 extensively penetrates this monolayer. A model of the organization of naRP2 in the presence of the DSPC monolayer is illustrated in Figure 6D. Furthermore, the much faster kinetics of the increase in the ellipsometric angle upon naRP2 binding in the presence of DSPC (Figure 6B) compared to that in the presence of DDPC (Figure 6A) suggests that a favorable interaction takes place between this protein and the saturated DSPC monolayer. The models shown in panels C and D of Figure 6 propose that naRP2 penetrates deeply into the DSPC monolayer with a high affinity whereas it remains at the surface of the DDPC monolayer; this is consistent with the MIP and synergy data obtained with these lipids (Figures 2A and 3A).

CONCLUSIONS

Biological membranes are very complex structures and correspond to a multicomponent chemical milieu in which species like proteins can be anchored. How this particular environment can modulate protein binding is of great interest. It is now well accepted that heterogeneities exist in membranes.[93,94] The importance of RP2 membrane binding for its function has been demonstrated on the basis of mutations that modify this interaction. This work highlights the particularly high affinity of naRP2 for saturated phospholipids, which are major components of lipid DRMs found in ROS membranes. In fact, the DRMs were found to be dramatically enriched in a phosphocholine mixture that is almost entirely saturated.[46] This affinity could be explained by the extensive penetration of naRP2 into the saturated DSPC monolayer even though a similar orientation of this protein was observed in the presence of saturated or polyunsaturated phospholipid monolayers. The role of RP2 acylation in its binding to microdomains is thus unclear. In this regard, the models in panels C and D of Figure 6 show that naRP2 is oriented with its N-terminus facing the membrane, which could allow its acyl groups to properly anchor the protein. One could also speculate that these acyl groups could prevent the extensive penetration of naRP2 in the presence of the DSPC monolayer. Such an extensive penetration of naRP2 in microdomains might then be responsible for the aberrant function of the nonacylated protein. Studies with acylated RP2 are therefore currently in progress to characterize its membrane binding and orientation compared to those of naRP2. These data shall provide useful information about the mechanism of action of this protein.

DOI: 10.1021/bi501517r
Biochemistry 2015, 54, 2560−2570

■ ASSOCIATED CONTENT

Supporting Information

Structure of human RP2 and PM-IRRAS spectra of a pure DSPC monolayer and naRP2 in the presence of a DSPC monolayer using a H_2O subphase. This material is available free of charge via the Internet at http://pubs.acs.org.

■ AUTHOR INFORMATION

Corresponding Author

*CUO-Recherche, Hôpital du Saint-Sacrement, Centre de recherche du CHU de Québec, Bureau K2-02, 1050 Chemin Ste-Foy, Québec, Québec, Canada G1S 4L8. Phone: 418-682-7569. Fax: 418-682-8000. E-mail: christian.salesse@fmed.ulaval.ca.

Funding

We are indebted to the Natural Sciences and Engineering Research Council of Canada (NSERC) for financial support. É.D. held a joint scholarship from the Canadian Institutes for Health Research (CIHR) and the E. A. Baker Foundation from the Canadian National Institute for the Blind. Moreover, É.D. also acknowledges a travel fellowship from the Réseau de recherche en santé de la vision. É.B. held a postdoctoral fellowship from the Fonds de Recherche du Québec-Santé (FRQ-S) as well as a Banting postdoctoral fellowship from the CIHR. H.H. held a postdoctoral fellowship from NSERC. P.C. was supported by a doctoral fellowship from the Regroupement stratégique PROTEO, which is funded by the Fonds de Recherche du Québec-Nature et Technologies (FRQNT).

Notes

The authors declare no competing financial interest.

■ REFERENCES

(1) Schwahn, U., Lenzner, S., Dong, J., Feil, S., Hinzmann, B., van Duijnhoven, G., Kirschner, R., Hemberger, M., Bergen, A. A. B., Rosenberg, T., Pinckers, A. J. L. G., Fundele, R., Rosenthal, A., Cremers, F. P. M., Ropers, H. H., and Berger, W. (1998) Positional cloning of the gene for X-linked retinitis pigmentosa 2. *Nat. Genet. 19*, 327−332.

(2) Kühnel, K., Veltel, S., Schlichting, I., and Wittinghofer, A. (2006) Crystal structure of the human retinitis pigmentosa 2 protein and its interaction with Arl3. *Structure 14*, 367−378.

(3) Bartolini, F., Bhamidipati, A., Thomas, S., Schwahn, U., Lewis, S. A., and Cowan, N. J. (2002) Functional overlap between retinitis pigmentosa 2 protein and the tubulin-specific chaperone cofactor C. *J. Biol. Chem. 277*, 14629−14634.

(4) Evans, R. J., Hardcastle, A. J., and Cheetham, M. E. (2006) Focus on molecules: X-linked Retinitis Pigmentosa 2 protein, RP2. *Exp. Eye Res. 82*, 543−544.

(5) Veltel, S., Gasper, R., Eisenacher, E., and Wittinghofer, A. (2008) The retinitis pigmentosa 2 gene product is a GTPase-activating protein for Arf-like 3. *Nat. Struct. Mol. Biol. 15*, 373−380.

(6) Zhang, H., Constantine, R., Vorobiev, S., Chen, Y., Seetharaman, J., Huang, Y. J., Xiao, R., Montelione, G. T., Gerstner, C. D., Davis, M. W., Inana, G., Whitby, F. G., Jorgensen, E. M., Hill, C. P., Tong, L., and Baehr, W. (2011) UNC119 is required for G protein trafficking in sensory neurons. *Nat. Neurosci. 14*, 874−880.

(7) Wright, K. J., Baye, L. M., Olivier-Mason, A., Mukhopadhyay, S., Sang, L., Kwong, M., Wang, W., Pretorius, P. R., Sheffield, V. C., Sengupta, P., Slusarski, D. C., and Jackson, P. K. (2011) An ARL3-UNC119-RP2 GTPase cycle targets myristoylated NPHP3 to the primary cilium. *Genes Dev. 25*, 2347−2360.

(8) Evans, R. J., Schwarz, N., Nagel-Wolfrum, K., Wolfrum, U., Hardcastle, A. J., and Cheetham, M. E. (2010) The retinitis pigmentosa protein RP2 links pericentriolar vesicle transport between the Golgi and the primary cilium. *Hum. Mol. Genet. 19*, 1358−1367.

(9) Karan, S., Zhang, H. B., Li, S., Frederick, J. M., and Baehr, W. (2008) A model for transport of membrane-associated phototransduction polypeptides in rod and cone photoreceptor inner segments. *Vision Res. 48*, 442−452.

(10) Schwarz, N., Hardcastle, A. J., and Cheetham, M. E. (2012) Arl3 and RP2 mediated assembly and traffic of membrane associated cilia proteins. *Vision Res. 75*, 2−4.

(11) Veltel, S., and Wittinghofer, A. (2009) RPGR and RP2: Targets for the treatment of X-linked retinitis pigmentosa? *Expert Opin. Ther. Targets 13*, 1239−1251.

(12) Zhang, H., Hanke-Gogokhia, C., Jiang, L., Li, X., Wang, P., Gerstner, C. D., Frederick, J. M., Yang, Z., and Baehr, W. (2015) Mistrafficking of prenylated proteins causes retinitis pigmentosa 2. *FASEB J. 29*, 932−942.

(13) Zhang, H. B., Hosier, S., Terew, J. M., Zhang, K., Cote, R. H., and Baehr, W. (2005) Assay and functional properties of PrBP(PDE delta), a prenyl-binding protein interacting with multiple partners. *Methods Enzymol. 403*, 42−56.

(14) Chapple, J. P., Hardcastle, A. J., Grayson, C., Spackman, L. A., Willison, K. R., and Cheetham, M. E. (2000) Mutations in the N-terminus of the X-linked retinitis pigmentosa protein RP2 interfere with the normal targeting of the protein to the plasma membrane. *Hum. Mol. Genet. 9*, 1919−1926.

(15) Evans, R. J., Chapple, J. P., Grayson, C., Hardcastle, A. J., and Cheetham, M. E. (2005) Assay and functional analysis of the ARL3 effector RP2 involved in X-linked retinitis pigmentosa. *Methods Enzymol. 404*, 468−480.

(16) Grayson, C., Bartolini, F., Chapple, J. P., Willison, K. R., Bhamidipati, A., Lewis, S. A., Luthert, P. J., Hardcastle, A. J., Cowan, N. J., and Cheetham, M. E. (2002) Localization in the human retina of the X-linked retinitis pigmentosa protein RP2, its homologue cofactor C and the RP2 interacting protein Arl3. *Hum. Mol. Genet. 11*, 3065−3074.

(17) Chapple, J. P., Grayson, C., Hardcastle, A. J., Bailey, T. A., Matter, K., Adamson, P., Graham, C. H., Willison, K. R., and Cheetham, M. E. (2003) Organization on the plasma membrane of the retinitis pigmentosa protein RP2: Investigation of association with detergent-resistant membranes and polarized sorting. *Biochem. J. 372*, 427−433.

(18) Chapple, J. P., Hardcastle, A. J., Grayson, C., Willison, K. R., and Cheetham, M. E. (2002) Delineation of the plasma membrane targeting domain of the X-linked retinitis pigmentosa protein RP2. *Invest. Ophthalmol. Visual Sci. 43*, 2015−2020.

(19) Schwahn, U., Paland, N., Techritz, S., Lenzner, S., and Berger, W. (2001) Mutations in the X-linked RP2 gene cause intracellular misrouting and loss of the protein. *Hum. Mol. Genet. 10*, 1177−1183.

(20) Breuer, D. K., Yashar, B. M., Filippova, E., Hiriyanna, S., Lyons, R. H., Mears, A. J., Asaye, B., Acar, C., Vervoort, R., Wright, A. F., Musarella, M. A., Wheeler, P., MacDonald, I., Iannaccone, A., Birch, D., Hoffman, D. R., Fishman, G. A., Heckenlively, J. R., Jacobson, S. G., Sieving, P. A., and Swaroop, A. (2002) A comprehensive mutation analysis of RP2 and RPGR in a North American cohort of families with X-linked retinitis pigmentosa. *Am. J. Hum. Genet. 70*, 1545−1554.

(21) Hardcastle, A. J., Thiselton, D. L., Van Maldergem, L., Saha, B. K., Jay, M., Plant, C., Taylor, R., Bird, A. C., and Bhattacharya, S. (1999) Mutations in the RP2 gene cause disease in 10% of families with familial X-linked retinitis pigmentosa assessed in this study. *Am. J. Hum. Genet. 64*, 1210−1215.

(22) Miano, M. G., Testa, F., Filippini, F., Trujillo, M., Conte, I., Lanzara, C., Millan, J. M., De Bernardo, C., Grammatico, B., Mangino, M., Torrente, I., Carrozzo, R., Simonelli, F., Rinaldi, E., Ventruto, V., D'Urso, M., Ayuso, C., and Ciccodicola, A. (2001) Identification of novel RP2 mutations in a subset of X-linked retinitis pigmentosa families and prediction of new domains. *Hum. Mutat. 18*, 109−119.

(23) Rosenberg, T., Schwahn, U., Feil, S., and Berger, W. (1999) Genotype-phenotype correlation in X-linked retinitis pigmentosa 2 (RP2). *Ophthalmic Genet. 20*, 161−172.

DOI: 10.1021/bi501517r
Biochemistry 2015, 54, 2560−2570

(24) Brockman, H. (1999) Lipid monolayers: Why use half a membrane to characterize protein-membrane interactions? *Curr. Opin. Struct. Biol. 9*, 438−443.
(25) Feng, S. S. (1999) Interpretation of Mechanochemical Properties of Lipid Bilayer Vesicles from the Equation of State or Pressure−Area Measurement of the Monolayer at the Air−Water or Oil−Water Interface. *Langmuir 15*, 998−1010.
(26) MacDonald, R. C., and Simon, S. A. (1987) Lipid monolayer states and their relationships to bilayers. *Proc. Natl. Acad. Sci. U.S.A. 84*, 4089−4093.
(27) Boucher, J., Trudel, E., Methot, M., Desmeules, P., and Salesse, C. (2007) Organization, structure and activity of proteins in monolayers. *Colloids Surf., B 58*, 73−90.
(28) Brezesinski, G., and Möhwald, H. (2003) Langmuir monolayers to study interactions at model membrane surfaces. *Adv. Colloid Interface Sci. 100−102*, 563−584.
(29) Calvez, P., Bussières, S., Demers, E., and Salesse, C. (2009) Parameters modulating the maximum insertion pressure of proteins and peptides in lipid monolayers. *Biochimie 91*, 718−733.
(30) Giner-Casares, J. J., Brezesinski, G., and Möhwald, H. (2014) Langmuir monolayers as unique physical models. *Curr. Opin. Colloid Interface Sci. 19*, 176−182.
(31) Kaganer, V. M., Mohwald, H., and Dutta, P. (1999) Structure and phase transitions in Langmuir monolayers. *Rev. Mod. Phys. 71*, 779−820.
(32) Maget-Dana, R. (1999) The monolayer technique: A potent tool for studying the interfacial properties of antimicrobial and membrane-lytic peptides and their interactions with lipid membranes. *Biochim. Biophys. Acta 1462*, 109−140.
(33) Moghaddam, B., Ali, M. H., Wilkhu, J., Kirby, D. J., Mohammed, A. R., Zheng, Q., and Perrie, Y. (2011) The application of monolayer studies in the understanding of liposomal formulations. *Int. J. Pharm. 417*, 235−244.
(34) Thakur, G., Micic, M., and Leblanc, R. M. (2009) Surface chemistry of Alzheimer's disease: A Langmuir monolayer approach. *Colloids Surf., B 74*, 436−456.
(35) Vollhardt, D., and Fainerman, V. B. (2000) Penetration of dissolved amphiphiles into two-dimensional aggregating lipid monolayers. *Adv. Colloid Interface Sci. 86*, 103−151.
(36) Blume, A., and Kerth, A. (2013) Peptide and protein binding to lipid monolayers studied by FT-IRRA spectroscopy. *Biochim. Biophys. Acta 1828*, 2294−2305.
(37) Casals, C., and Canadas, O. (2012) Role of lipid ordered/disordered phase coexistence in pulmonary surfactant function. *Biochim. Biophys. Acta 1818*, 2550−2562.
(38) Koller, D., and Lohner, K. (2014) The role of spontaneous lipid curvature in the interaction of interfacially active peptides with membranes. *Biochim. Biophys. Acta 1838*, 2250−2259.
(39) Lhor, M., Bernier, S. C., Horchani, H., Bussieres, S., Cantin, L., Desbat, B., and Salesse, C. (2014) Comparison between the behavior of different hydrophobic peptides allowing membrane anchoring of proteins. *Adv. Colloid Interface Sci. 207*, 223−239.
(40) Stefaniu, C., Brezesinski, G., and Mohwald, H. (2014) Langmuir monolayers as models to study processes at membrane surfaces. *Adv. Colloid Interface Sci. 208*, 197−213.
(41) Fliesler, S. J., and Anderson, R. E. (1983) Chemistry and metabolism of lipids in the vertebrate retina. *Prog. Lipid Res. 22*, 79−131.
(42) N'Soukpoé-Kossi, C. N., Salesse, C., Leblanc, R. M., and Boucher, F. (1985) Molar absorptivities of bovine retina rod outer segment phospholipids in n-hexane. *Anal. Biochem. 151*, 409−417.
(43) Miljanich, G. P., Sklar, L. A., White, D. L., and Dratz, E. A. (1979) Disaturated and dipolyunsaturated phospholipids in the bovine retinal rod outer segment disk membrane. *Biochim. Biophys. Acta 552*, 294−306.
(44) Gordon, W. C., and Bazan, N. G. (1990) Docosahexaenoic acid utilization during rod photoreceptor cell renewal. *J. Neurosci. 10*, 2190−2202.
(45) Rodriguez de Turco, E. B., Gordon, W. C., and Bazan, N. G. (1994) Docosahexaenoic acid is taken up by the inner segment of frog photoreceptors leading to an active synthesis of docosahexaenoyl-inositol lipids: Similarities in metabolism in vivo and in vitro. *Curr. Eye Res. 13*, 21−28.
(46) Martin, R. E., Elliott, M. H., Brush, R. S., and Anderson, R. E. (2005) Detailed characterization of the lipid composition of detergent-resistant membranes from photoreceptor rod outer segment membranes. *Invest. Ophthalmol. Visual Sci 46*, 1147−1154.
(47) Elliott, M. H., Nash, Z. A., Takemori, N., Fliesler, S. J., McClellan, M. E., and Naash, M. I. (2008) Differential distribution of proteins and lipids in detergent-resistant and detergent-soluble domains in rod outer segment plasma membranes and disks. *J. Neurochem. 104*, 336−352.
(48) Yang, W., Di Vizio, D., Kirchner, M., Steen, H., and Freeman, M. R. (2010) Proteome scale characterization of human S-acylated proteins in lipid raft-enriched and non-raft membranes. *Mol. Cell. Proteomics 9*, 54−70.
(49) Yamazaki, A., Bondarenko, V. A., Matsuura, I., Tatsumi, M., Kurono, S., Komori, N., Matsumoto, H., Hayashi, F., Yamazaki, R. K., and Usukura, J. (2010) Mechanism for the regulation of mammalian cGMP phosphodiesterase 6. 1: Identification of its inhibitory subunit complexes and their roles. *Mol. Cell. Biochem. 339*, 215−233.
(50) Calvez, P., Demers, E., Boisselier, E., and Salesse, C. (2011) Analysis of the contribution of saturated and polyunsaturated phospholipid monolayers to the binding of proteins. *Langmuir 27*, 1373−1379.
(51) Boisselier, E., Calvez, P., Demers, E., Cantin, L., and Salesse, C. (2013) Effect of oxidation of polyunsaturated phospholipids on the binding of proteins in monolayers. *Colloids Surf., B 109*, 109−114.
(52) Boisselier, E., Calvez, P., Demers, E., Cantin, L., and Salesse, C. (2012) Influence of the physical state of phospholipid monolayers on protein binding. *Langmuir 28*, 9680−9688.
(53) Lavoie, H., Desbat, B., Vaknin, D., and Salesse, C. (2002) Structure of rhodopsin in monolayers at the air-water interface: A PM-IRRAS and X-ray reflectivity study. *Biochemistry 41*, 13424−13434.
(54) Gallant, J., Desbat, B., Vaknin, D., and Salesse, C. (1998) Polarization-modulated infrared spectroscopy and X-ray reflectivity of photosystem II core complex at the gas-water interface. *Biophys. J. 75*, 2888−2899.
(55) Blaudez, D., Buffeteau, T., Cornut, J. C., Desbat, B., Escafre, N., Pezolet, M., and Turlet, J. M. (1993) Polarization-modulated FT-IR spectroscopy of a spread monolayer at the air-water-interface. *Appl. Spectrosc. 47*, 869−874.
(56) Buffeteau, T., and Desbat, B. (1989) Thin-film optical-constants determined from infrared reflectance and transmittance measurements. *Appl. Spectrosc. 43*, 1027−1032.
(57) Berreman, D. W. (1972) Optics in stratified and anisotropic media: 4 × 4-matrix formulation. *J. Opt. Soc. Am. 62*, 502−510.
(58) Belbachir, K., Lecomte, S., Ta, H. P., Petibois, C., and Desbat, B. (2011) Orientation of molecular groups of fibers in nonoriented samples determined by polarized ATR-FTIR spectroscopy. *Anal. Bioanal. Chem. 401*, 3263−3268.
(59) Buffeteau, T., Calvez, E. L., Castano, S., Desbat, B., Blaudez, D., and Dufourcq, J. (2000) Anisotropic Optical Constants of α-Helix and β-Sheet Secondary Structures in the Infrared. *J. Phys. Chem. B 104*, 4537−4544.
(60) Arrondo, J. L., Muga, A., Castresana, J., and Goni, F. M. (1993) Quantitative studies of the structure of proteins in solution by Fourier-transform infrared spectroscopy. *Prog. Biophys. Mol. Biol. 59*, 23−56.
(61) Barth, A. (2007) Infrared spectroscopy of proteins. *Biochim. Biophys. Acta 1767*, 1073−1101.
(62) Barth, A., and Zscherp, C. (2002) What vibrations tell us about proteins. *Q. Rev. Biophys. 35*, 369−430.
(63) Goormaghtigh, E., Cabiaux, V., and Ruysschaert, J. M. (1994) Determination of soluble and membrane protein structure by Fourier transform infrared spectroscopy. III. Secondary structures. *Subcell. Biochem. 23*, 405−450.

DOI: 10.1021/bi501517r
Biochemistry 2015, 54, 2560−2570

(64) Jackson, M., and Mantsch, H. H. (1995) The use and misuse of FTIR spectroscopy in the determination of protein structure. *Crit. Rev. Biochem. Mol. Biol. 30*, 95−120.
(65) Manning, M. C. (2005) Use of infrared spectroscopy to monitor protein structure and stability. *Exp. Rev. Proteomics 2*, 731−743.
(66) Renault, A., Rioux-Dube, J. F., Lefevre, T., Pezennec, S., Beaufils, S., Vie, V., Tremblay, M., and Pezolet, M. (2009) Surface properties and conformation of *Nephila clavipes* spider recombinant silk proteins at the air-water interface. *Langmuir 25*, 8170−8180.
(67) Salesse, C., Ducharme, D., Leblanc, R. M., and Boucher, F. (1990) Estimation of disk membrane lateral pressure and molecular area of rhodopsin by the measurement of its orientation at the nitrogen-water interface from an ellipsometric study. *Biochemistry 29*, 4567−4575.
(68) Verger, R., and Pattus, F. (1982) Lipid-protein interactions in monolayers. *Chem. Phys. Lipids 30*, 189−227.
(69) De Grip, W. J., Daemen, F. J., and Bonting, S. L. (1980) Isolation and purification of bovine rhodopsin. *Methods Enzymol. 67*, 301−320.
(70) Silvius, J. R. (2003) Role of cholesterol in lipid raft formation: Lessons from lipid model systems. *Biochim. Biophys. Acta 1610*, 174−183.
(71) Marsh, D. (1996) Lateral pressure in membranes. *Biochim. Biophys. Acta 1286*, 183−223.
(72) Schroeder, R., London, E., and Brown, D. (1994) Interactions between Saturated Acyl Chains Confer Detergent Resistance on Lipids and Glycosylphosphatidylinositol (GPI)-Anchored Proteins: GPI-Anchored Proteins in Liposomes and Cells Show Similar Behavior. *Proc. Natl. Acad. Sci. U.S.A. 91*, 12130−12134.
(73) Boguslavsky, V., Rebecchi, M., Morris, A. J., Jhon, D. Y., Rhee, S. G., and Mclaughlin, S. (1994) Effect of monolayer surface pressure on the activities of phosphoinositide-specific phospholipase-C-β-1, phospholipase-C-γ-1, and phospholipase-C-δ-1. *Biochemistry 33*, 3032−3037.
(74) Moreau, H., Pieroni, G., Jolivetreynaud, C., Alouf, J. E., and Verger, R. (1988) A new kinetic approach for studying phospholipase-C (*Clostridium perfringens* α-toxin) activity on phospholipid monolayers. *Biochemistry 27*, 2319−2323.
(75) Seelig, A. (1987) Local-anesthetics and pressure: A comparison of dibucaine binding to lipid monolayers and bilayers. *Biol. Chem. Hoppe-Seyler 368*, 1272.
(76) Blume, A., and Eibl, H. (1979) Influence of charge on bilayer membranes: Calorimetric investigations of phosphatidic-acid bilayers. *Biochim. Biophys. Acta 558*, 13−21.
(77) Demel, R. A., Geurtsvankessel, W. S. M., Zwaal, R. F. A., Roelofsen, B., and Vandeenen, L. L. M. (1975) Relation between various phospholipase actions on human red-cell membranes and interfacial phospholipid pressure in monolayers. *Biochim. Biophys. Acta 406*, 97−107.
(78) Mendelsohn, R., Mao, G., and Flach, C. R. (2010) Infrared reflection-absorption spectroscopy: Principles and applications to lipid-protein interaction in Langmuir films. *Biochim. Biophys. Acta 1798*, 788−800.
(79) Blaudez, D., Buffeteau, T., Desbat, B., and Turlet, J.-M. (1999) Infrared and Raman spectroscopies of monolayers at the air−water interface. *Curr. Opin. Colloid Interface Sci. 4*, 265−272.
(80) Fabian, H., and Mantele, W. (2002) Infrared Spectroscopy of Proteins. *Handbook of vibrational spectroscopy*, Vol. 5, pp 3399−3425, Wiley, New York.
(81) Blaudez, D., Castano, S., and Desbat, B. (2011) PM-IRRAS at liquid interfaces. *Biointerface characterization by advanced IR spectroscopy*, Chapter 2, pp 27−55, Wiley, New York.
(82) Castano, S., Desbat, B., Laguerre, M., and Dufourcq, J. (1999) Structure, orientation and affinity for interfaces and lipids of ideally amphipathic lytic LiKj (i=2j) peptides. *Biochim. Biophys. Acta 1416*, 176−194.
(83) Flach, C. R., Brauner, J. W., Taylor, J. W., Baldwin, R. C., and Mendelsohn, R. (1994) External reflection FTIR of peptide monolayer films in-situ at the air/water interface: Experimental-design, spectra-structure correlations, and effects of hydrogen-deuterium exchange. *Biophys. J. 67*, 402−410.
(84) Khurana, R., and Fink, A. L. (2000) Do parallel β-helix proteins have a unique Fourier transform infrared spectrum? *Biophys. J. 78*, 994−1000.
(85) Grandbois, M., Desbat, B., and Salesse, C. (2000) Monitoring of phospholipid monolayer hydrolysis by phospholipase A2 by use of polarization-modulated Fourier transform infrared spectroscopy. *Biophys. Chem. 88*, 127−135.
(86) Barth, A. (2000) The infrared absorption of amino acid side chains. *Prog. Biophys. Mol. Biol. 74*, 141−173.
(87) Desmeules, P., Penney, S. E., Desbat, B., and Salesse, C. (2007) Determination of the contribution of the myristoyl group and hydrophobic amino acids of recoverin on its dynamics of binding to lipid monolayers. *Biophys. J. 93*, 2069−2082.
(88) Lavoie, H., Blaudez, D., Vaknin, D., Desbat, B., Ocko, B. M., and Salesse, C. (2002) Spectroscopic and structural properties of valine gramicidin A in monolayers at the air-water interface. *Biophys. J. 83*, 3558−3569.
(89) Banc, A., Desbat, B., Renard, D., Popineau, Y., Mangavel, C., and Navailles, L. (2007) Structure and orientation changes of ω- and γ-gliadins at the air-water interface: A PM-IRRAS spectroscopy and Brewster angle microscopy study. *Langmuir 23*, 13066−13075.
(90) Cornut, I., Desbat, B., Turlet, J. M., and Dufourcq, J. (1996) In situ study by polarization modulated Fourier transform infrared spectroscopy of the structure and orientation of lipids and amphipathic peptides at the air-water interface. *Biophys. J. 70*, 305−312.
(91) Ducharme, D., Max, J. J., Salesse, C., and Leblanc, R. M. (1990) Ellipsometric study of the physical states of phosphatidylcholines at the air-water interface. *J. Phys. Chem. B 94*, 1925−1932.
(92) Trudel, E., Beaufils, S., Renault, A., Breton, R., and Salesse, C. (2006) Binding of RPE65 fragments to lipid monolayers and identification of its partners by glutathione S-transferase pull-down assays. *Biochemistry 45*, 3337−3347.
(93) Fan, J., Sammalkorpi, M., and Haataja, M. (2010) Formation and regulation of lipid microdomains in cell membranes: Theory, modeling, and speculation. *FEBS Lett. 584*, 1678−1684.
(94) Lingwood, D., and Simons, K. (2010) Lipid rafts as a membrane-organizing principle. *Science 327*, 46−50.

DOI: 10.1021/bi501517r
Biochemistry 2015, 54, 2560−2570